ACS Photonics

pubs.acs.org/journal/apchd5

Article

Femtosecond Time-Resolved Infrared-Resonant Third-Order Sum-Frequency Spectroscopy

Jizhou Wang, Kai Wang,* Yujie Shen, Zehua Han, Fu Li, Zhe He, Da-wei Wang, Alexei V. Sokolov,* and Marlan O. Scully

Cite This: *ACS Photonics* 2021, 8, 1137−1142

Read Online

ACCESS | Metrics & More | Article Recommendations | Supporting Information

ABSTRACT: We demonstrate a coherent vibrational spectroscopy based on molecular infrared (IR)-active resonance. We apply two femtosecond pulses (one in near-IR and the other in mid-IR) to generate the femtosecond time-resolved IR-resonant third-order sum-frequency signal. The mid-IR pulse is tuned to be resonant with molecular vibrations. This experimental configuration converts the IR light into a visible signal and exhibits high sensitivity to the vibrational mode of the molecule. The technique can be applied to acquire chemical information on various biological samples, including living tissues in their natural water-rich state. This approach can also be used to study the dynamics of IR-active vibrational modes, that is, measure the decoherence time.

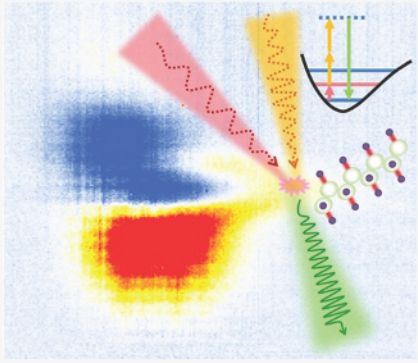

KEYWORDS: *midinfrared spectroscopy, third-order nonlinearity, sum-frequency generation, molecular dynamics, decoherence time*

Midinfrared (MIR) radiation with wavelengths from 3 to 20 μm can resonate with vibrational and rotational molecular transitions. This range includes the vibrational "fingerprint" region that can be used for spectroscopic identification of molecules. Fourier-transform infrared (FTIR) spectroscopy, based on the Michelson interferometer, is a widely used MIR technique. Compared to the traditional spectroscopy using dispersive spectrometers, FTIR can obtain the absorption or emission MIR spectra with high sensitivity and spectral resolution,[1] which makes it an effective method for the identification and classification of materials, determining the purity of compounds, and detecting the interaction of samples with the environment such as the oxidation process at the molecular level.[2−6] On the other hand, FTIR has the following drawbacks: (1) it is hard to be implemented in samples with water, such as living cells, because water has strong and broad absorption in the MIR region, which can obscure the FTIR signal; (2) the FTIR spectroscopy has a long acquisition time that hinders the detection of fast dynamics; (3) it measures the absorption signal contributed by all the molecules, and thus, it falls short of depth resolution; (4) it requires IR detectors such as the mercury cadmium telluride (MCT) detector, which is more expensive and less efficient than detectors working in the visible range.

To tackle these problems, several new types of MIR spectroscopies have been developed. For example, the MIR dual-comb spectroscopy can dramatically reduce the amount of time for data acquistion.[7−9] Photothermal spectroscopy usually utilizes a near-infrared (NIR) or visible light to probe the photothermal effect caused by the resonance absorption. It can detect samples in aqueous environments and provides depth resolution.[10−13] Another approach is to convert the MIR light into the NIR or visible light via nonlinear optical effects.[14−28] Previous research has proposed a video-rate, mid-infrared hyperspectral up-conversion imaging of biological tissues using a lithium niobite crystal to convert a picosecond (ps) MIR pulse to a NIR pulse.[15] However, this method requires an additional second-order nonlinear crystal for the up-conversion process. An alternative way is to use the nonlinearity of the sample, in which the nonlinear optical conversion and IR absorption can share the same transition.[16−25] In this case, the nonlinear processes are sensitive to the vibrational modes and provide vibrational specification in the visible range. The experimental setups are simplified and promoted with a higher spatial resolution. Compared with IR light, the visible signal has less loss in the watery materials. In principle, this property guarantees a deeper penetration depth. The resonant second-order sum-frequency generation spectroscopy has been used with one resonant MIR pulse and one nonresonant pulse to generate the sum-frequency signal.[22−24] The signal is usually in

Received: December 22, 2020
Published: February 12, 2021

the NIR or visible region that can be easily detected by using a Si-based detector. Because the second-order nonlinear process is forbidden in centrosymmetric materials, this sum-frequency signal is usually generated on surfaces, interfaces, and noncentrosymmetric materials. To extend the applications of the IR sum-frequency spectroscopy, third-order nonlinear spectroscopy have been developed.[16,17,25]

Here we develop a femtosecond time-resolved IR-resonant third-order sum-frequency (ITS) spectroscopy where a visible photon of the signal is generated by absorbing a resonant MIR photon plus two off-resonance NIR photons, as shown in Figure 1. The resonant MIR absorption at the frequency ω_{MIR}

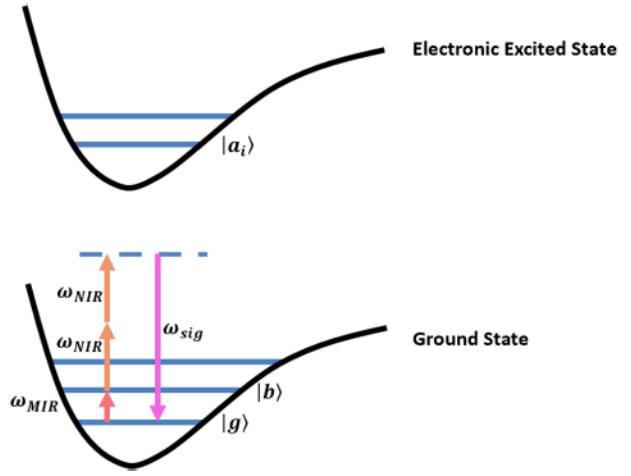

Figure 1. Schematic energy levels and transitions of the femtosecond time-resolved IR-resonant third-order sum-frequency (ITS) spectroscopy. The red arrow represents one MIR photon at the frequency of ω_{MIR}, which is resonant with the transition between the ground state $|g\rangle$ and the excited state $|b\rangle$. The two orange arrows (ω_{NIR}) denote two NIR photons with a frequency ω_{NIR}. The green line arrow is the IRS signal at the frequency of $\omega_{sig} = \omega_{MIR} + 2\omega_{NIR}$.

can result in a coherence between ground state $|g\rangle$ and excited state $|b\rangle$. The near light ω_{NIR} probes the coherence and generates a third-order nonlinear signal through a two photon process. The ITS signal is generated at the frequency $\omega_{sig} = \omega_{MIR} + 2\omega_{NIR}$. However, a nonresonant four-wave-mixing (FWM) signal at the same wavelength accompanies the ITS signal when the MIR and NIR pulses overlap, which distorts the ITS signal and makes it difficult to be extracted. ITS signals usually can be separated from FWM background by adding a proper time delay, because the nonresonant FWM signal requires the exact overlap of the input pulses, while ITS signals decay with the coherence of vibrational states. This approach can overcome several issues that plague the traditional MIR spectroscopy. First, for the samples that contain water, the nonlinear process can happen within the IR penetration depth and generates visible signals that are in the transparency window of water. Second, ITS does not require a long acquisition time due to the resonant process and the large IR absorption cross-section. Third, the nonlinear signal can provide depth resolution that, thanks to the nonlinear signal generation process, requires strong input intensities that can only be achieved at the focus volume. Finally, the visible signal can be detected with high efficiency using Si detectors. Although phase mismatching limits the nonlinear process, it is not a problem in the tight-focusing configuration or when a thin sample is studied.

ITS spectroscopy can be compared with the coherent anti-Stokes Raman spectroscopy (CARS). Both of them are third-order nonlinear processes, and their output signals contain nonresonant FWM background, which can be suppressed by adding delays between pulses. CARS is sensitive to Raman active modes, but ITS spectroscopy probes IR-active vibrational modes, which are complementary to Raman modes and have a larger cross section. In addition, ITS uses a simpler experimental setup that only uses two beams (the MIR pump and the NIR probe) instead of three in CARS (pump, Stokes, and probe). The wavelength of the ITS signal is in the visible range, which is much easier to be separated from the fundamental IR beams.

RESULTS

Figure 2a shows the experiment setup. The MIR and NIR pulses were generated by two separate Optical Parametric Amplifiers (OPAs; OPerA Solo kHz OPA, Coherent Co.), which were pumped by pulses from a femtosecond (fs) amplifier (Astrella, 1 kHz, 75 fs, 7.5 W, Coherent Co.). To prepare coherent excitation, the wavelength of the MIR pulse

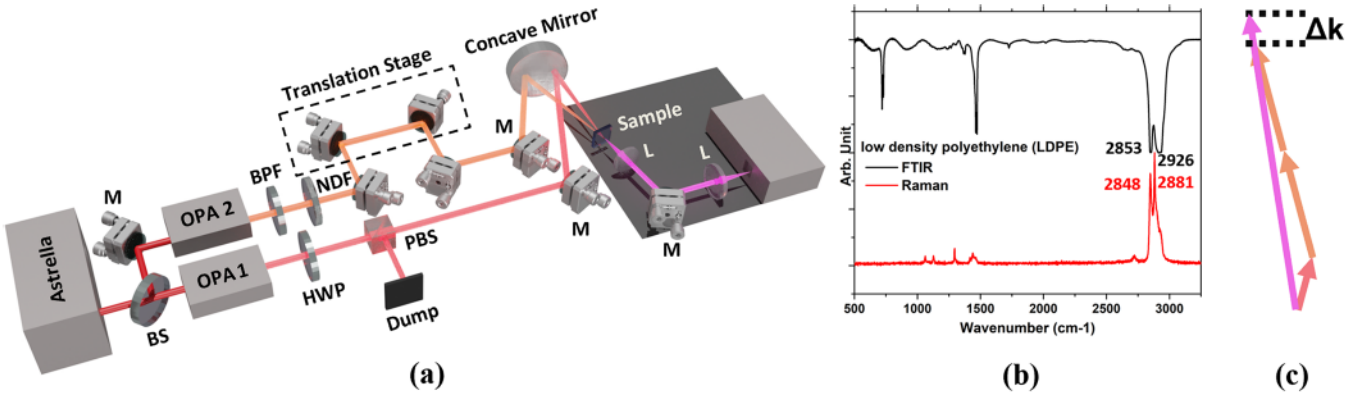

Figure 2. (a) Setup of the femtosecond time-resolved ITS spectroscopy. The MIR pump beam (red) generated from "OPA 1" and the NIR probe beam (orange) from "OPA 2" are focused by a concave mirror with a 100 cm focus length on the sample. The ITS signal generated on the sample is measured by the spectrometer. M: mirror. BS: beam splitter. BPF: bandpass filter. NDF: neutral density filter. HWP: half wave plate. PBS: polarizing beam splitter. L: lens. (b) FT-IR (black) and Raman (red) spectra of low-density polyethylene (LDPE). The four peaks corresponding to the CH_2 band.[4,29] (c) Wavevector diagram of the two IR beams and the ITS signal. Δk is the wavevector mismatch.

https://dx.doi.org/10.1021/acsphotonics.0c01940
ACS Photonics 2021, 8, 1137−1142

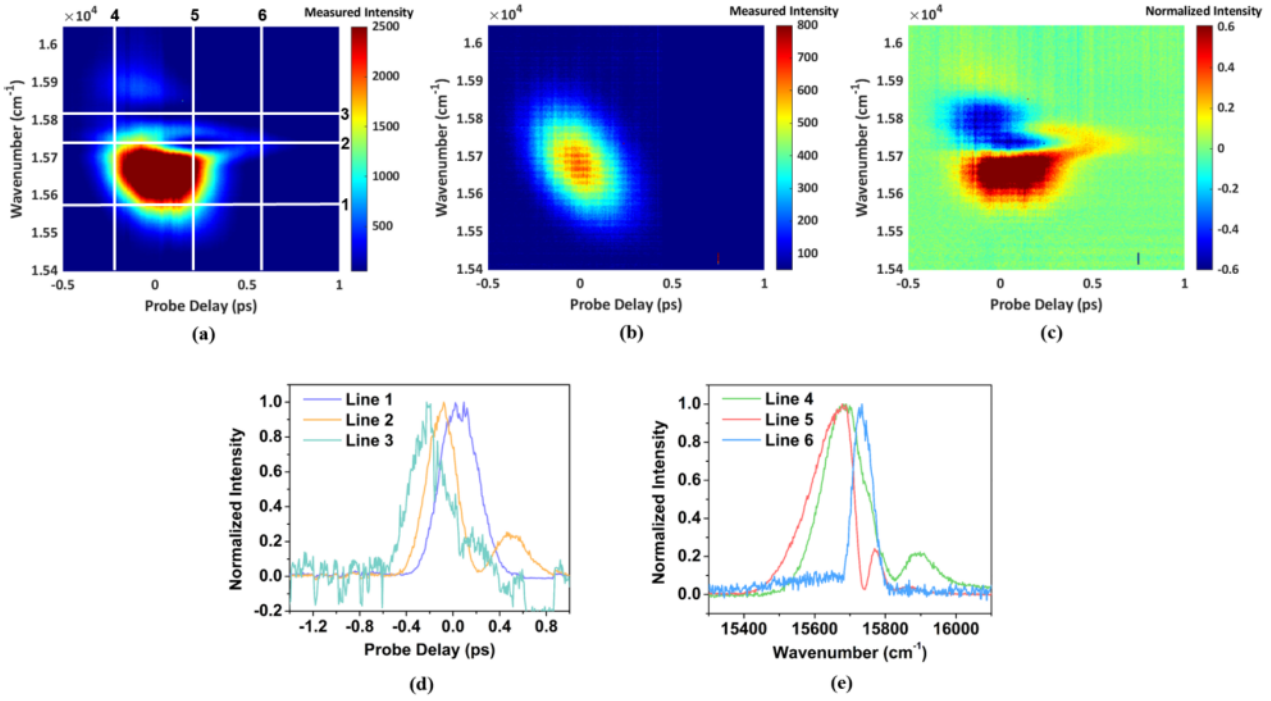

Figure 3. (a) *X*-axis is the delay time between the NIR and MIR pulses. The zero probe delay is the time estimated when the two pulses overlap. *Y*-axis is the wavenumber of the visible signal. Each vertical line on the diagram represents a spectrum measured at the delay time *x*. (b) 2D spectrum of the nonresonant FWM generated on the coverslip. (c) 2D spectrum of the FWM generated on the LDPE film after subtracting the nonresonant FWM background. Both (a) and (b) are normalized at 15579 cm^{-1}, then use (b) and subtract (a). (d) Three normalized signal intensity lines change with the time delay at different signal wavenumbers, as shown in (a). Line 1 corresponds to 15579 cm^{-1}; Line 2 corresponds to 15739 cm^{-1}; Line 3 corresponds to 15811 cm^{-1}. (e) Three normalized signal spectra of the film at different time delays in (a). Line 4 is the spectrum at the probe delay time −0.21 ps; line 5 is at the delay time 0.23 ps; Line 6 is at the delay time 0.59 ps.

was tuned near-resonant with the vibrational modes of the sample. A half-wave plate for 3.5 μm (WPLQ05M-3500, Thorlabs Co.) and a polarization beam splitter (BDY12, Thorlabs Co.) were used to control the power of the MIR beam. The NIR pulse centered at 1550 nm was sent through a delay stage. To increase the spectral resolution of the ITS, we used a bandpass filter centered at 1550 nm (FB1550-12, Thorlabs Co.) to narrow the bandwidth down to 12 nm and stretched the pulse duration to about 350 fs. To avoid burning the sample but maintain high signal to noice ratio, the powers of the MIR and NIR pulses were tuned to about 16 and 17 μJ, respectively. The two IR pulses were focused on the sample by a spherical mirror (f = 100 cm, CM508-1000-P01, Thorlabs) with a small incidence angle (about 0.9°) difference. The long focal length provided a large focus spot to generate a strong signal. The visible ITS signal was generated in the sample and emitted in a different direction from the two input beams due to the phase-matching condition. The ITS signal was collected by a spectrometer (Chromatix, Andor Co.) with 0.25 nm resolution (6.2 cm^{-1}).

We used a low-density polyethylene (LDPE, 13 μm, Glad ClingWrap, Glad Co.) film as the sample. Figure 2b shows the Raman and FTIR spectra of the LDPE film. The peaks at 2853 and 2926 cm^{-1} in the FTIR spectrum and 2848 and 2881 cm^{-1} in the Raman spectrum are assigned to the CH_2 stretching.[4,29] To excite the vibrational modes, we set the center wavelength of the MIR beam as 3460 nm (2890 cm^{-1}). The broadband MIR pulse can cover both the 2853 and 2926 cm^{-1} peaks. The wavelength of the ITS signal was around 634 nm, which corresponds to around 1.58×10^4 cm^{-1}.

The third-order nonlinear susceptibility[30] is

$$\chi^{(3)} = \frac{2N}{4\pi\varepsilon_0\hbar^3}\sum_i\sum_j \frac{\mu_{ga_i}\mu_{a_ia_i'}\mu_{a_ib}\mu_{bg}\rho_{gg}^{(0)}}{(\omega_{bg}-\omega_{\mathrm{MIR}})+i\Gamma_1}\times\left[\frac{1}{(\omega_{a_ib}-\omega_{\mathrm{NIR}})+i\Gamma_2}\cdot\frac{1}{(\omega_{a_ib}-2\omega_{\mathrm{NIR}})+i\Gamma_3}+\frac{1}{(\omega_{a_ib}+\omega_{\mathrm{NIR}}+i\Gamma_2)(\omega_{a_ib}+2\omega_{\mathrm{NIR}}+i\Gamma_3)}\right]$$

where a, b, and g are the energy levels in Figure 1, i and j are sum for different vibrational modes, Γ_i is the spontaneous decay rate, and μ_{ij} is the transition dipole moment. This third-order nonlinear process requires phase matching. However, for most materials with normal dispersion, the wavevector mismatch Δk shown in Figure 2c is nonzero. To generate the nonlinear signal, the sample thickness Δl needs to be small,

$$\Delta k\cdot\Delta l \le \pi$$

which results in $\Delta l \le 26$ μm for the LDPE film, and our sample is within this range.

In Figure 3a, we show the 2D spectrum of the output signal generated on a LDPE film by scanning the time delay between the NIR and MIR pulses with 6.7 fs step sizes. The acquisition time at each step was set to be 0.5 s. To indicate an apparent difference in the signal of the CH_2 vibrational modes in the LDPE film from the nonresonant FWM background, a comparison measurement of glass coverslips (150 μm in thickness) were carried out under the same condition with the acquisition time of 2 s (shown in Figure 3b). Here, only the nonresonant FWM due to the NIR and MIR pulses was observed, which means the coverslip has no IR absorption in the spectral region near 3460 nm. In Figure 3a it contains the

https://dx.doi.org/10.1021/acsphotonics.0c01940
ACS Photonics 2021, 8, 1137−1142

ITS signal resulting from the CH_2 vibrational states as well as the nonresonant FWM background. The nonresonant FWM background was removed from the 2D spectrum of the LDPE film by the subtraction between the normalized 2D spectra of the LDPE film and the coverslip (Figure 3c). We noticed that when the NIR and MIR pulses overlapped in space and time, two absorptions emerged around 15739 cm^{-1} (line 2) and 15811 cm^{-1} (line 3) with a 72 cm^{-1} difference. They matched with the 2853 and 2926 cm^{-1} peaks in the FTIR spectra. We observed that the output signal decreases rather than increases when the FWM background and the ITS signals are generated simultaneously. Other groups have reported similar phenomena with the second-order sum-frequency spectroscopy,[18,24] where the authors claimed that the dips resulted from the destructive interference between the sum-frequency signal and the nonresonant FWM background. We have a simulation in the Supporting Information considering the absorption and prepulse effect. The original spectra of lines 1, 2, and 3 in Figure 3a are shown in Figure 3d. Along line 2, we notice that a "tail" emerges after the two IR pulses are separated around 0.5 ps, then gradually declines to zero as the delay is increased. It is the ITS signal generated from the 2853 cm^{-1} vibrational state. The decoherence time of the 2926 cm^{-1} vibrational state is so short that the ITS signal generated from this state, which is supposed to be another "tail" around line 3, can barely be measured in this case. Figure 3e shows the spectra at different probe delay times. The position of the dip on line 5 matches with the peak of line 6, which is the ITS signal generated from the 2853 cm^{-1} vibrational state. The spectrum of line 6 illustrates that, by tuning the probe delay at 0.59 ps, only the ITS signal from the vibrational state is generated, which means only the molecules with the targeted IR-active vibrational mode can generate the signal. It is ideal for chemical imaging without further data process.

The decay rate of the ITS signal reflects the decoherence of the excited vibrational state. We summed all the signal intensities in the tail region and then plotted the integrated intensity as a function of the probe delay time, as shown in Figure 4. The fitting result exhibits the exponential time constant is about 150 fs, which shows a subps decoherence time of polymer materials at room temperature.

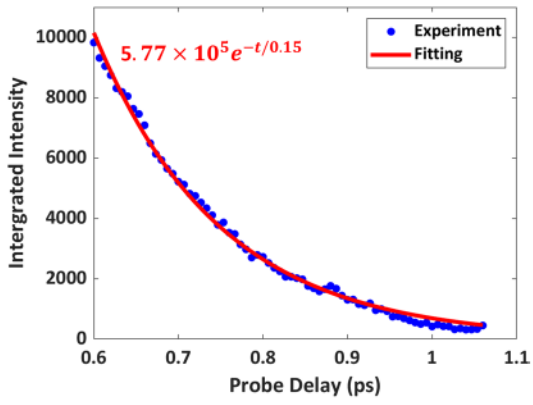

Figure 4. Integrated intensity as a function of probe delay time. The intensity is integrated from 15680 to 15790 cm^{-1}, covering the whole region of the tail signal in Figure 3b. The blue dots are the experimental data; the red line is the exponential decay fitting.

DISCUSSION

By combining different types of microscopy, our method can also be applied in scanning microscopy and wide-field microscopy for label-free imaging. By setting the delay time at 0.6 ps in this experiment, we can suppress the nonresonant FWM signal and keep the ITS signal, which can be used for spectral imaging. This approach provides a high spatial resolution and breaks the diffraction limit of the two IR input beams. According to the Abbe diffraction limit $d = \frac{\lambda}{2NA}$ (NA is the numerical aperture), ITS has a higher spatial resolution, which is several times higher than that of MIR due to the shorter wavelength λ. Moreover, compared to IR spectroscopy, measurement with visible light benefits from the commercially available high NA objectives. Take the data in this experiment, for example, the wavelength λ is about 634 nm, with a water immersion objective (NA = 1.20), the diffraction limit is $d \sim 265$ nm. It has been shown that 0.45 μm resolution can be achieved with a picosecond laser source in biological samples at zero time-delay.[16,17] The spatial resolution can be improved by tuning the probe beam to a shorter wavelength.

The strong absorption of IR can induce the thermal effect at room temperature, which has been used in photothermal spectroscopy.[10−13] This experiment was conducted below the thermal damage threshold. Since we use 1 kHz laser system, heat accumulation is very weak. Another possible influence is the deformation of the film and the thermally induced fluctuation of the refractive index. According to our observation, these effects have a negligible impact on the collection of the ITS signal.

The time-resolved ITS spectroscopy provides the spectral information as well as decoherence of vibrational states with a femtosecond temporal resolution. The decoherence time of certain states is important and fundamental in many fields, such as alignment of molecules,[31,32] remote atmospheric lasing,[33,34] quantum lithography,[35,36] superradiance,[37−42] and quantum information.[43] In principle, the ITS technique can be extended to study chemical reactions, molecular structure, environmental dynamics, phonon dynamics, and phonon−exciton coupling in low-dimensional materials. ITS can be a complementary technique to two-dimensional infrared spectroscopy.[44]

CONCLUSION

In summary, we have developed a coherent time-resolved vibrationally sensitive spectroscopic technique that combines IR-resonant excitation with convenient signal detection in the visible frequency range. We provide an experimental demonstration of the femtosecond time-resolved ITS spectroscopy by recording a 2D spectrum of the LDPE film. This technique allows us to measure IR-active modes instead of Raman-active modes. It can be considered as a complementary technique to CARS. Moreover, this experiment exhibited that the nonresonant FWM background could be suppressed by adding proper pulse delays, which is ideal for chemical imaging without any extra data processing. On top of that, the time-resolved ITS spectroscopy provides a new way of measuring the dynamics of the vibrational states at the molecular level, like the dynamics of coherence exhibited in this experiment. It has potential applications, including studying the dynamics of relaxation, chemical reactions, molecular structure, environ-

https://dx.doi.org/10.1021/acsphotonics.0c01940
ACS Photonics 2021, 8, 1137−1142

mental dynamics, phonon dynamics, and phonon−exciton coupling, in low-dimensional materials.

■ ASSOCIATED CONTENT

Supporting Information

The Supporting Information is available free of charge at https://pubs.acs.org/doi/10.1021/acsphotonics.0c01940.

2D spectrum simulation (PDF)

■ AUTHOR INFORMATION

Corresponding Authors

Kai Wang − *Institute for Quantum Science and Engineering, Texas A&M University, College Station, Texas 77840, United States; School of Physics and Astronomy, Sun Yat-sen University, Zhuhai, Guangdong 519082, China;* Email: wangk289@mail.sysu.edu.cn

Alexei V. Sokolov − *Institute for Quantum Science and Engineering, Texas A&M University, College Station, Texas 77840, United States; Baylor Research Innovative Center, Baylor University, Waco, Texas 76798, United States;* Email: sokol@tamu.edu

Authors

Jizhou Wang − *Institute for Quantum Science and Engineering, Texas A&M University, College Station, Texas 77840, United States; Interdisciplinary Center for Quantum Information and State Key Laboratory of Modern Optical Instrumentation, Zhejiang Province Key Laboratory of Quantum Technology and Device, and Department of Physics, Zhejiang University, Hangzhou, Zhejiang 310027, China;* orcid.org/0000-0003-2605-7278

Yujie Shen − *Institute for Quantum Science and Engineering, Texas A&M University, College Station, Texas 77840, United States*

Zehua Han − *Institute for Quantum Science and Engineering, Texas A&M University, College Station, Texas 77840, United States*

Fu Li − *Institute for Quantum Science and Engineering, Texas A&M University, College Station, Texas 77840, United States*

Zhe He − *Institute for Quantum Science and Engineering, Texas A&M University, College Station, Texas 77840, United States; Department of Medical Engineering, California Institute of Technology, Pasadena, California 91125, United States;* orcid.org/0000-0002-8525-3650

Da-wei Wang − *Interdisciplinary Center for Quantum Information and State Key Laboratory of Modern Optical Instrumentation, Zhejiang Province Key Laboratory of Quantum Technology and Device, and Department of Physics, Zhejiang University, Hangzhou, Zhejiang 310027, China; Zhejiang Laboratory, Hangzhou, Zhejiang 311121, China*

Marlan O. Scully − *Institute for Quantum Science and Engineering, Texas A&M University, College Station, Texas 77840, United States; Baylor Research Innovative Center, Baylor University, Waco, Texas 76798, United States*

Complete contact information is available at: https://pubs.acs.org/10.1021/acsphotonics.0c01940

Author Contributions

J.W., Y.S., K.W., and A.V.S. designed the experiment. J.W., K.W., Y.S., Z.H., F.L., and Z.H., performed the experiment. J.W., K.W., D.W., A.V.S., and M.O.S. analyzed the results. A.V.S. and M.O.S. supervised the project. J.W. wrote the paper with input from all authors.

Notes

The authors declare no competing financial interest.

■ ACKNOWLEDGMENTS

We thank Prof. Volker Deckert for the useful discussion. We gratefully acknowledge the support from the Office of Naval Research (Award Nos. N00014-16-1-2578 and N00014-20-1-2184), the Robert A. Welch Foundation (Grant Nos. A-1261 and A-1547), National Science Foundation (Grant No. PHY-2013771), the Air Force Office of Scientific Research (Award No. FA9550-20-1-0366 DEF), the National Natural Science Foundation of China (Grant No. 11934011), the Major Scientific Research Project of Zhejiang Lab (Nos. 2019MB0AD01 and 20190057), and Fundamental Research Funds for the Central Universities of China. Z.H., F.L., and Z.H. were supported by the Herman F. Heep and Minnie Belle Heep Texas A&M University Endowed Fund held/administered by the Texas A&M Foundation.

■ REFERENCES

(1) Smith, B. C. *Fundamentals of Fourier Transform Infrared Spectroscopy*, 2nd ed.; CRC Press: London, England, 2011; pp 12−16.

(2) Vlachos, N.; Skopelitis, Y.; Psaroudaki, M.; Konstantinidou, V.; Chatzilazarou, A.; Tegou, E. Applications of Fourier Transform-Infrared Spectroscopy to Edible Oils. *Anal. Chim. Acta* **2006**, *573−574*, 459−465.

(3) Lerma-García, M. J.; Ramis-Ramos, G.; Herrero-Martínez, J. M.; Simó-Alfonso, E. F. Authentication of Extra Virgin Olive Oils by Fourier-Transform Infrared Spectroscopy. *Food Chem.* **2010**, *118* (1), 78−83.

(4) Koenig, J. L. Application of Fourier Transform Infrared Spectroscopy to Chemical Systems. *Appl. Spectrosc.* **1975**, *29* (4), 293−308.

(5) *Infrared Spectroscopy of Biomolecules*; Mantsch, H. H., Chapman, D., Eds.; John Wiley & Sons: Nashville, TN, 1996; pp 19−38.

(6) Helm, D.; Labischinski, H.; Schallehn, G.; Naumann, D. Classification and Identification of Bacteria by Fourier-Transform Infrared Spectroscopy. *J. Gen. Microbiol.* **1991**, *137* (1), 69−79.

(7) Coddington, I.; Newbury, N.; Swann, W. Dual-Comb Spectroscopy. *Optica* **2016**, *3* (4), 414.

(8) Ycas, G.; Giorgetta, F. R.; Baumann, E.; Coddington, I.; Herman, D.; Diddams, S. A.; Newbury, N. R. High-Coherence Mid-Infrared Dual-Comb Spectroscopy Spanning 2.6 to 5.2 Mm. *Nat. Photonics* **2018**, *12* (4), 202−208.

(9) Yu, M.; Okawachi, Y.; Griffith, A. G.; Picqué, N.; Lipson, M.; Gaeta, A. L. Silicon-Chip-Based Mid-Infrared Dual-Comb Spectroscopy. *Nat. Commun.* **2018**, *9* (1), na.

(10) Bialkowski, S. E.; Mandelis, A. Photothermal Spectroscopy Methods for Chemical Analysis. *Phys. Today* **1996**, *49* (10), 76−76.

(11) Aamodt, L. C.; Murphy, J. C. Thermal Effects in Photothermal Spectroscopy and Photothermal Imaging. *J. Appl. Phys.* **1983**, *54* (2), 581−591.

(12) Zhang, D.; Li, C.; Zhang, C.; Slipchenko, M. N.; Eakins, G.; Cheng, J.-X. Depth-Resolved Mid-Infrared Photothermal Imaging of Living Cells and Organisms with Submicrometer Spatial Resolution. *Sci. Adv.* **2016**, *2* (9), e1600521.

(13) Mertiri, A.; Altug, H.; Hong, M. K.; Mehta, P.; Mertz, J.; Ziegler, L. D.; Erramilli, S. Nonlinear Midinfrared Photothermal Spectroscopy Using Zharov Splitting and Quantum Cascade Lasers. *ACS Photonics* **2014**, *1* (8), 696−702.

(14) Kalashnikov, D. A.; Paterova, A. V.; Kulik, S. P.; Krivitsky, L. A. Infrared Spectroscopy with Visible Light. *Nat. Photonics* **2016**, *10* (2), 98−101.

(15) Junaid, S.; Chaitanya Kumar, S.; Mathez, M.; Hermes, M.; Stone, N.; Shepherd, N.; Ebrahim-Zadeh, M.; Tidemand-Lichtenberg, P.; Pedersen, C. Video-Rate, Mid-Infrared Hyperspectral Upconversion Imaging. *Optica* **2019**, *6* (6), 702.
(16) Hanninen, A. M.; Prince, R. C.; Potma, E. Triple Modal Coherent Nonlinear Imaging with Vibrational Contrast. *IEEE J. Sel. Top. Quantum Electron.* **2018**, 1−1.
(17) Hanninen, A. M.; Prince, R. C.; Ramos, R.; Plikus, M. V.; Potma, E. O. High-Resolution Infrared Imaging of Biological Samples with Third-Order Sum-Frequency Generation Microscopy. *Biomed. Opt. Express* **2018**, *9* (10), 4807−4817.
(18) Koelsch, P.; Muglali, M.; Rohwerder, M.; Erbe, A. Third-Order Effects in Resonant Sum-Frequency-Generation Signals at Electrified Metal/Liquid Interfaces. *J. Opt. Soc. Am. B* **2013**, *30* (1), 219.
(19) Morrow, D. J.; Kohler, D. D.; Zhao, Y.; Jin, S.; Wright, J. C. Triple Sum Frequency Pump-Probe Spectroscopy of Transition Metal Dichalcogenides. *Phys. Rev. B* **2019**, *100* (23), 235303.
(20) Boyle, E. S.; Neff-Mallon, N. A.; Wright, J. C. Triply Resonant Sum Frequency Spectroscopy: Combining Advantages of Resonance Raman and 2D-IR. *J. Phys. Chem. A* **2013**, *117* (47), 12401−12408.
(21) Boyle, E. S.; Pakoulev, A. V.; Wright, J. C. Fully Coherent Triple Sum Frequency Spectroscopy of a Benzene Fermi Resonance. *J. Phys. Chem. A* **2013**, *117* (27), 5578−5588.
(22) Shen, Y. R. Surface Properties Probed by Second-Harmonic and Sum-Frequency Generation. *Nature* **1989**, *337* (6207), 519−525.
(23) Richter, L. J.; Petralli-Mallow, T. P.; Stephenson, J. C. Vibrationally Resolved Sum-Frequency Generation with Broad-Bandwidth Infrared Pulses. *Opt. Lett.* **1998**, *23* (20), 1594−1596.
(24) Lagutchev, A.; Hambir, S. A.; Dlott, D. D. Nonresonant Background Suppression in Broadband Vibrational Sum-Frequency Generation Spectroscopy. *J. Phys. Chem. C* **2007**, *111* (37), 13645−13647.
(25) Bonn, M.; Hess, C.; Miners, J. H.; Heinz, T. F.; Bakker, H. J.; Cho, M. Novel Surface Vibrational Spectroscopy: Infrared-Infrared-Visible Sum-Frequency Generation. *Phys. Rev. Lett.* **2001**, *86* (8), 1566−1569.
(26) Fishman, D. A.; Cirloganu, C. M.; Webster, S.; Padilha, L. A.; Monroe, M.; Hagan, D. J.; Van Stryland, E. W. Sensitive Mid-Infrared Detection in Wide-Bandgap Semiconductors Using Extreme Non-Degenerate Two-Photon Absorption. *Nat. Photonics* **2011**, *5* (9), 561−565.
(27) Hayat, A.; Ginzburg, P.; Orenstein, M. Infrared Single-Photon Detection by Two-Photon Absorption in Silicon. *Phys. Rev. B: Condens. Matter Mater. Phys.* **2008**, *77* (12), na.
(28) Knez, D.; Hanninen, A. M.; Prince, R. C.; Potma, E. O.; Fishman, D. A. Infrared Chemical Imaging through Non-Degenerate Two-Photon Absorption in Silicon-Based Cameras. *Light: Sci. Appl.* **2020**, *9* (1), 125.
(29) Lin-Vien, D.; Colthup, N. B.; Fateley, W. G.; Grasselli, J. G. *Handbook of Infrared and Raman Characteristic Frequencies of Organic Molecules*; Academic Press, 2014; p 12.
(30) Boyd, R. W. *Nonlinear Opt.*; Academic Press: San Diego, CA, *1991*, 2008; pp 180−185.
(31) Stapelfeldt, H. Alignment of Molecules by Strong Laser Pulses. *Eur. Phys. J. D* **2003**, *26* (1), 15−19.
(32) Yao, J.; Chu, W.; Liu, Z.; Chen, J.; Xu, B.; Cheng, Y. An Anatomy of Strong-Field Ionization-Induced Air Lasing. *Appl. Phys. B: Lasers Opt.* **2018**, *124* (5), na.
(33) Yuan, L.; Liu, Y.; Yao, J.; Cheng, Y. Recent Advances in Air Lasing: A Perspective from Quantum Coherence. *Adv. Quantum Technol.* **2019**, *2* (11), 1900080.
(34) Yuan, L.; Hokr, B. H.; Traverso, A. J.; Voronine, D. V.; Rostovtsev, Y.; Sokolov, A. V.; Scully, M. O. Theoretical Analysis of the Coherence-Brightened Laser in Air. *Phys. Rev. A: At., Mol., Opt. Phys.* **2013**, *87* (2), na.
(35) Liao, Z.; Al-Amri, M.; Zubairy, M. S. Quantum Lithography beyond the Diffraction Limit via Rabi Oscillations. *Phys. Rev. Lett.* **2010**, *105* (18), 183601.
(36) Liao, Z.; Al-Amri, M.; Zubairy, M. S. Coherent Rabi Oscillations in a Molecular System and Sub-Diffraction-Limited Pattern Generation. *J. Phys. B: At., Mol. Opt. Phys.* **2015**, *48* (10), 105101.
(37) Zhang, A.; Wang, L.; Chen, X.; Yakovlev, V. V.; Yuan, L. Tunable Super- and Subradiant Boundary States in One-Dimensional Atomic Arrays. *Commun. Phys.* **2019**, *2* (1), na.
(38) Svidzinsky, A. A.; Li, F.; Li, H.; Zhang, X.; Ooi, C. H. R.; Scully, M. O. Single-Photon Superradiance and Radiation Trapping by Atomic Shells. *Phys. Rev. A: At., Mol., Opt. Phys.* **2016**, *93* (4), na.
(39) Rossatto, D. Z.; Pires, D. P.; de Paula, F. M.; de Sá Neto, O. P. Quantum Coherence and Speed Limit in the Mean-Field Dicke Model of Superradiance. *Phys. Rev. A* **2020**, *102* (5), 053716.
(40) Xia, H.; Svidzinsky, A. A.; Yuan, L.; Lu, C.; Suckewer, S.; Scully, M. O. Observing Superradiant Decay of Excited-State Helium Atoms inside Helium Plasma. *Phys. Rev. Lett.* **2012**, *109* (9), 093604.
(41) Harries, J. R.; Iwayama, H.; Kuma, S.; Iizawa, M.; Suzuki, N.; Azuma, Y.; Inoue, I.; Owada, S.; Togashi, T.; Tono, K.; Yabashi, M.; Shigemasa, E. Superfluorescence, Free-Induction Decay, and Four-Wave Mixing: Propagation of Free-Electron Laser Pulses through a Dense Sample of Helium Ions. *Phys. Rev. Lett.* **2018**, *121* (26), 263201.
(42) Wang, K.; Wang, Y.; Wang, J.; Yi, Z.; Kulatilaka, W. D.; Sokolov, A. V.; Scully, M. O. Femtosecond Pump-Probe Studies of Atomic Hydrogen Superfluorescence in Flames. *Appl. Phys. Lett.* **2020**, *116* (20), 201102.
(43) Schlosshauer, M. Decoherence, the Measurement Problem, and Interpretations of Quantum Mechanics. *Rev. Mod. Phys.* **2005**, *76* (4), 1267−1305.
(44) Stone, K. W.; Gundogdu, K.; Turner, D. B.; Li, X.; Cundiff, S. T.; Nelson, K. A. Two-Quantum 2D FT Electronic Spectroscopy of Biexcitons in GaAs Quantum Wells. *Science* **2009**, *324* (5931), 1169−1173.

https://dx.doi.org/10.1021/acsphotonics.0c01940
ACS Photonics 2021, 8, 1137−1142